PHYSICAL REVIEW B **84**, 085318 (2011)

Polarized and resonant Raman spectroscopy on single InAs nanowires

M. Möller,* M. M. de Lima Jr., and A. Cantarero
Materials Science Institute, University of Valencia, P.O. Box 22085, E-46071 Valencia, Spain

L. C. O. Dacal
Instituto de Estudos Avançados (IEAv), CTA, São José dos Campos, São Paulo, Brazil

J. R. Madureira
Faculdade de Ciências Integradas do Pontal, Universidade Federal de Uberlândia (UFU), Ituiutaba-MG, Brazil

F. Iikawa, T. Chiaramonte, and M. A. Cotta
Instituto de Física Gleb Wataghin, UNICAMP, CP 6165, 13083-970 Campinas, São Paulo, Brazil
(Received 15 April 2011; revised manuscript received 13 July 2011; published 26 August 2011)

We report polarized Raman scattering and resonant Raman scattering studies on single InAs nanowires. Polarized Raman experiments show that the highest scattering intensity is obtained when both the incident and analyzed light polarizations are perpendicular to the nanowire axis. InAs wurtzite optical modes are observed. The obtained wurtzite modes are consistent with the selection rules and also with the results of calculations using an extended rigid-ion model. Additional resonant Raman scattering experiments reveal a redshifted E_1 transition for InAs nanowires compared to the bulk zinc-blende InAs transition due to the dominance of the wurtzite phase in the nanowires. *Ab initio* calculations of the electronic band structure for wurtzite and zinc-blende InAs phases corroborate the observed values for the E_1 transitions.

DOI: 10.1103/PhysRevB.84.085318 PACS number(s): 78.67.Uh, 78.30.Fs

I. INTRODUCTION

Semiconductor nanowires have a very promising potential for the next generation of advanced optoelectronic devices.[1,2] Among the several unique properties of semiconductor nanowires, one can highlight the possibility of an epitaxial growth in the wurtzite or zinc-blende phases, or a combination of both (ideally zinc-blende/wurtzite superlattices). In bulk form, most of the III-V materials (phosphides, arsenides, and antimonides) crystallize in the cubic zinc-blende structure, while for the nitrides the stable phase is the wurtzite. In contrast, the nanowires may exhibit an intermixing of zinc blende and wurtzite. The transition between both phases corresponds to a modification in the stacking sequence along the direction of one of the bonds (the [111] direction in the case of the zinc-blende structure or the [0001] direction in the wurtzite structure). Since the band structure of the zinc-blende and wurtzite structures differs for the same material,[3,4] the optoelectronic properties of the nanowires are dependent on their structural composition. In this sense, Raman spectroscopy is a powerful nondestructive tool that enables the investigation of the structural, electronic, and optical properties of a nanowire. In particular, it provides access to the phonon modes near the center of the Brillouin zone (first-order Raman scattering) as well as information on the electronic transitions (resonant Raman scattering).

Among the III-V compounds, InAs has emerged as a narrow-band-gap semiconductor with very high electron mobility and a small electron effective mass,[5] which is particularly convenient for high-frequency electronic applications.[6] While bulk InAs crystallizes in cubic zinc-blende structure, it has been demonstrated that InAs nanowires can be grown in the wurtzite form.[7–10] In this paper, we use first-order polarized Raman scattering and resonant Raman scattering to investigate single InAs nanowires. First-order polarized Raman scattering have been recently used to investigate GaN,[11,12] GaAs,[13,14] GaP,[15] ZnO,[16] RuO_2,[17] and CdS (Ref. 18) single one-dimensional nanostructures. However, to the best of our knowledge, there are no previous polarized Raman data regarding InAs nanowires in the literature so far. In addition, we have observed a redshifted E_1 energy transition for the InAs nanowires as well as a surface optical (SO) phonon mode.

The paper is organized as follows: In Sec. II, the nanowire growth and the experimental details related with the Raman scattering setup are presented. In Sec. III, we review the selection rules for the first-order Raman scattering from bulk InAs and compare it with our experiments on bulk InAs. In Sec. IV, the selection rules for the particular cases of the zinc-blende and wurtzite nanowires grown in the [111] and [0001] direction, respectively, are considered and compared with the experimental polarized Raman scattering results from single InAs nanowires. These measurements agree with the phonon energies and two-phonon density of states calculated with an extended rigid-ion model. In addition, the observation of an SO phonon mode is presented; finally, an *ab initio* calculation of the electronic band structure of wurtzite and zinc-blende InAs and the experimental resonant Raman scattering results are compared and discussed in Sec. V.

II. EXPERIMENTAL

The investigated InAs nanowires have been grown by the vapor liquid solid method in a chemical beam epitaxy system using gold nanoparticles as catalysts on an (100) GaAs substrate. Growth precursors are trimethyl indium [$(CH_3)_3In$] diluted with hydrogen (H_2) as a carrier gas, and thermally

decomposed arsine (AsH_3). The growth temperature of the InAs nanowires is 480 °C.

The structure of the nanowires has been studied by transmission electron microscopy (TEM) in a representative set of nanowires belonging to the same CBE-grown sample. The TEM images show nanowires with a rodlike shape, with diameters in the range of 40–200 nm and lengths of 5–15 μm. The nanowires exhibit an intermixture of zinc-blende and wurtzite phase and are grown along the [111] and [0001] direction, respectively. The particular nanowire discussed in this paper has a diameter in the range of 70–80 nm as measured by atomic force microscopy (AFM).

Raman spectroscopy was performed in a μ-Raman setup in the backscattering configuration on single InAs nanowires mechanically transferred onto a GaAs substrate coated with a 1-μm-thick Al layer. The metal film was used to block the background signal from the GaAs substrate to provide the visual contrast between nanowires and the substrate surface and to dissipate the heat produced by the laser. The lines of an Ar/Kr ion laser were used for excitation at a relatively low laser power (~600 μW). The scattered light was dispersed by a Jobin Yvon T64000 spectrometer and detected with a liquid-nitrogen-cooled charge-coupled device. In order to perform polarization-dependent measurements, the incident light passes through a $\lambda/2$ plate so that its polarization $\hat{e}_i$ can be rotated by an angle ϕ with respect to the growth axis of the nanowire. Before being focused on the nanowire by a 50× objective, the light passes a beam splitter. In addition, an analyzer—set either parallel or perpendicular to the nanowire axis—was used to filter the polarization of the scattered light $\hat{e}_s$. Equivalent experiments with a fixed incident polarization and a rotatable analyzer were also performed and give the same results, as expected due to symmetry. A schematic diagram of the setup is shown in Fig. 1. Two coordinate systems are introduced: the laboratory coordinates system (x,y,z) and the crystal coordinates system of the nanowire (x_1',x_2',x_3'). z and x_3' are parallel to the growth axis of the nanowire while x_1' is rotated by an angle (θ) with respect to the x axis in the x-y plane.

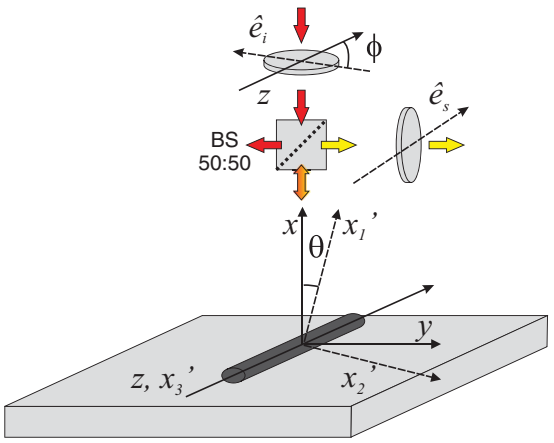

FIG. 1. (Color online) Schematic diagram of the experimental setup and the used coordinate systems (x,y,z) and (x_1',x_2',x_3') in backscattering geometry. $\hat{e}_i$ and $\hat{e}_s$ are the incident and scattered light polarizations, respectively.

III. RAMAN SCATTERING ON BULK InAs

The *nonresonant* Raman scattered intensity (I_s) depends on the polarization of the incident radiation ($\hat{e}_i$), the polarization of the scattered radiation ($\hat{e}_s$), and the Raman tensor $\mathcal{R}$, which is related to the crystal symmetry, as[19]

$$I_s \propto \omega^4 |\hat{e}_i \cdot \mathcal{R} \cdot \hat{e}_s|^2, \tag{1}$$

where ω is the angular frequency of the scattered light. For zinc-blende crystal optical phonons polarized along the directions $\hat{e}_1 = (100) \parallel x$, $\hat{e}_2 = (010) \parallel y$, or $\hat{e}_3 = (001) \parallel z$, their Raman tensors $\mathcal{R}_{e_1}$, $\mathcal{R}_{e_2}$, and $\mathcal{R}_{e_3}$ can be represented by a (3 × 3) matrix with nonzero elements d,

$$\mathcal{R}_{e_1} = \begin{pmatrix} 0 & 0 & 0 \\ 0 & 0 & d \\ 0 & d & 0 \end{pmatrix}, \quad \mathcal{R}_{e_2} = \begin{pmatrix} 0 & 0 & d \\ 0 & 0 & 0 \\ d & 0 & 0 \end{pmatrix}, \quad \mathcal{R}_{e_3} = \begin{pmatrix} 0 & d & 0 \\ d & 0 & 0 \\ 0 & 0 & 0 \end{pmatrix}, \tag{2}$$

respectively. In the zinc-blende structure, the zone-center optical phonons split into two transverse-optical (TO) modes and a longitudinal-optical (LO) mode. Note that, due to the macroscopic longitudinal electric field, the Raman tensor elements d are different for the TO and the LO mode.

If we consider, for example, the (100) and the (111) surfaces, then the LO mode can be observed in backscattering configuration on both surfaces, whereas the TO mode is only allowed in backscattering from the (111) surface.

In this work, we investigated single InAs nanowires grown in the [111] (zinc-blende) or [0001] (wurtzite) direction. Starting from the zinc-blende structure, we set

$$\hat{x}_1' = T^{-1}\hat{e}_1 = \frac{1}{\sqrt{6}}[1,1,\bar{2}], \quad \hat{x}_2' = T^{-1}\hat{e}_2 = \frac{1}{\sqrt{2}}[\bar{1},1,0],$$
$$\text{and} \quad \hat{x}_3' = T^{-1}\hat{e}_3 = \frac{1}{\sqrt{3}}[1,1,1],$$

representing the basis of the nanowire crystal coordinate system. In order to calculate the selection rules for the zinc-blende structure, the Raman tensors are transformed in two steps. First, the Raman tensors are transformed into the laboratory coordinate system with basis $\{\hat{e}_1,\hat{e}_2,\hat{e}_3\}$. Secondly, they are rotated around the z axis by the angle θ (see Fig. 1) in order to account for the additional degree of freedom of the top surface of the nanowires. The two transformations can be described by the matrices

$$T = \begin{pmatrix} \frac{1}{\sqrt{6}} & \frac{1}{\sqrt{6}} & -\frac{2}{\sqrt{6}} \\ -\frac{1}{\sqrt{2}} & \frac{1}{\sqrt{2}} & 0 \\ \frac{1}{\sqrt{3}} & \frac{1}{\sqrt{3}} & \frac{1}{\sqrt{3}} \end{pmatrix}, \quad S = \begin{pmatrix} \cos\theta & -\sin\theta & 0 \\ \sin\theta & \cos\theta & 0 \\ 0 & 0 & 1 \end{pmatrix}, \tag{3}$$

where T denotes the transformation into the basis $\{\hat{e}_1,\hat{e}_2,\hat{e}_3\}$ and S is the rotation about the nanowire axis z. For reasons of simplicity, we define $M = ST$. The Raman tensors $R_{x_i'}$ for displacements along the directions x_i' in the basis $\{\hat{e}_1,\hat{e}_2,\hat{e}_3\}$

can now be written as

$$\mathcal{R}_{x_i'} = \sum_{j=1}^{3} M_{ij}\mathcal{R}_{e_j}, \quad i = 1,2,3, \tag{4}$$

and the Raman tensors $\tilde{\mathcal{R}}_{x_i'}$ in the basis $\{\hat{x}_1',\hat{x}_2',\hat{x}_3'\}$ can be described by

$$\tilde{\mathcal{R}}_{x_i'} = M\mathcal{R}_{x_i'}M^T, \quad i = 1,2,3. \tag{5}$$

Here, we have considered a backscattering configuration along the x axis. In laboratory coordinates, the polarization $\hat{e}_i$ of the incident radiation and the polarization $\hat{e}_s$ of the scattered light take the form (see Fig. 1)

$$\hat{e}_i = \begin{pmatrix} 0 \\ \sin\phi \\ \cos\phi \end{pmatrix}, \quad \hat{e}_s^{\perp} = \begin{pmatrix} 0 \\ 1 \\ 0 \end{pmatrix}, \quad \hat{e}_s^{\parallel} = \begin{pmatrix} 0 \\ 0 \\ 1 \end{pmatrix}, \tag{6}$$

depending on whether the scattered radiation is analyzed perpendicular ($\hat{e}_s^{\perp}$) or parallel ($\hat{e}_s^{\parallel}$) to the wire axis, respectively. By inserting the obtained Raman tensors [Eq. (5)] in Eq. (1), the Raman intensities of the zinc-blende structure for different configurations can be obtained. In Fig. 2, the theoretical intensities of the scattered light polarized perpendicular ($I_{\perp}$, polarized in the y direction) or parallel ($I_{\parallel}$, polarized in the z direction) to the [111] direction as a function of the angle ϕ of the incident polarization with respect to [111] are shown for TO (a) and LO phonons (b) from an InAs bulk substrate (110) in polar plots taking into account only the contribution of the Raman tensors. For perpendicular analysis ($I_{\perp}$), the maximum intensity of the TO mode is obtained for an angle of the incident polarization of 63°, while for the parallel analyzed polarization ($I_{\parallel}$) the maximum intensity is found for 0° with respect to the [111] direction. The LO mode is only allowed in $I_{\perp}$ and the highest intensity is reached for 90°. As a reference, we performed polarized Raman scattering on a bulk InAs (110) substrate. The polar patterns for the experimental results of the TO and LO phonon are shown in Figs. 2(c) and 2(d), respectively. The experimental data show good agreement with the theory. The small shifts of the TO and LO intensity maxima of about 8° and 4°, respectively, are attributed to an inclination of the polarization direction of the light with respect to the crystallographic axes of the substrate. Note that the selection rule for the LO mode in perpendicular analysis ($I_{\perp}$) is not fulfilled. This is attributed to the fact that the laser excitation energy (2.41 eV) is close to the E_1 Raman transition of InAs bulk (2.57 eV), which provokes the appearance of the forbidden LO mode.[20]

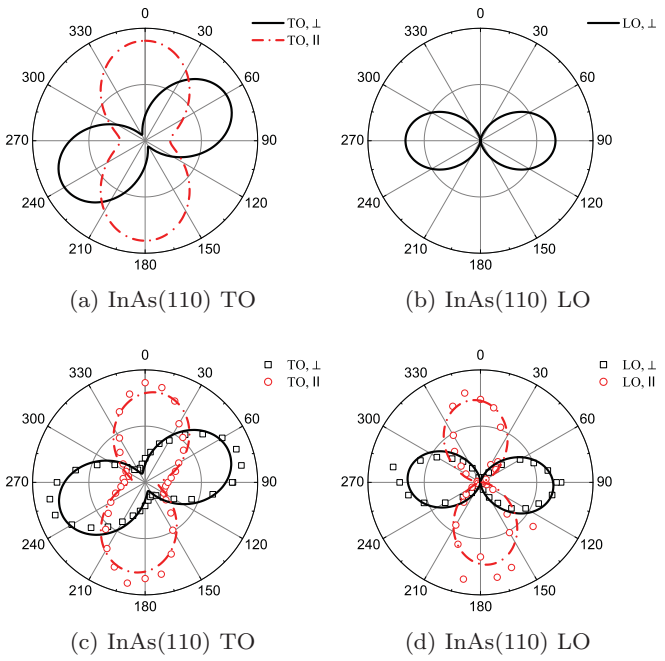

(a) InAs(110) TO (b) InAs(110) LO

(c) InAs(110) TO (d) InAs(110) LO

FIG. 2. (Color online) Calculated intensity polar patterns of the scattered light polarized perpendicular ($I_{\perp}$) or parallel ($I_{\parallel}$) to the [111] direction as a function of the angle ϕ of the incident polarization with respect to [111] are shown for TO (a) and LO (b) phonons in backscattering from an InAs (110) bulk substrate. The LO intensity is zero for parallel analysis (∥). Measured polarized Raman scattering of the TO (c) and the LO mode (d) on a reference bulk InAs (110) substrate excited with the 514.5 nm excitation line. Open squares and circles represent the experimental Raman scattering intensities for perpendicular ($I_{\perp}$) and parallel ($I_{\parallel}$) analysis with respect to the [111] direction. Solid and dashed curves are squared cosine fits to the data.

IV. RAMAN SCATTERING ON ZINC-BLENDE AND WURTZITE NANOWIRES

In this section, we focus on the Raman scattering on zinc-blende and wurtzite nanowires. First, we consider theoretically the polarization dependence of wurtzite and zinc-blende nanowires; then we present the experimental polarized Raman scattering result; finally, we address the SO mode observed in the Raman spectra (Fig. 5).

A. Theoretical considerations on zinc-blende and wurtzite nanowires

In order to calculate the polar patterns of I_s for nanowires, one has to take care of the additional degree of freedom associated with the rotation of θ around the nanowire axis since it can influence the polar patterns of the optical modes. In the following, we address the polar patterns of zinc-blende and wurtzite nanowires grown along the [111] and [0001] direction, respectively.

For zinc-blende InAs nanowires grown in the [111] direction, the TO modes for a parallel analyzer (∥) and the LO mode do not depend on θ and are identical to the ones shown in Fig. 2. However, the TO mode for a perpendicular analyzer (⊥) does vary with θ, as illustrated in Fig. 3. Note that the polar pattern presents a periodicity of 120°, and that, although the polar pattern is circular (i.e., independent of the incident polarization) for $\theta = N \times 60°(N = 0,1,2\ldots)$, for any other angle the scattering is polarized. The maximum scattering intensity is dependent on both the rotational angle θ and the polarization angle ϕ. Note that the highest intensities are obtained for polarization angles $\phi_{\max}$ different from 0° and 90° (for example, $45° < \phi_{\max} < 63°$ for $60° < \theta < 120°$). This angular dependence is a clear signature of the presence of zinc-blende TO modes and can be used for their assignation.

The phonon dispersion of the wurtzite phase along the [0001] direction can be approximated by simply folding the Brillouin zone of the zinc-blende phase along the [111] direction since the unit cell of the zinc-blende structure is

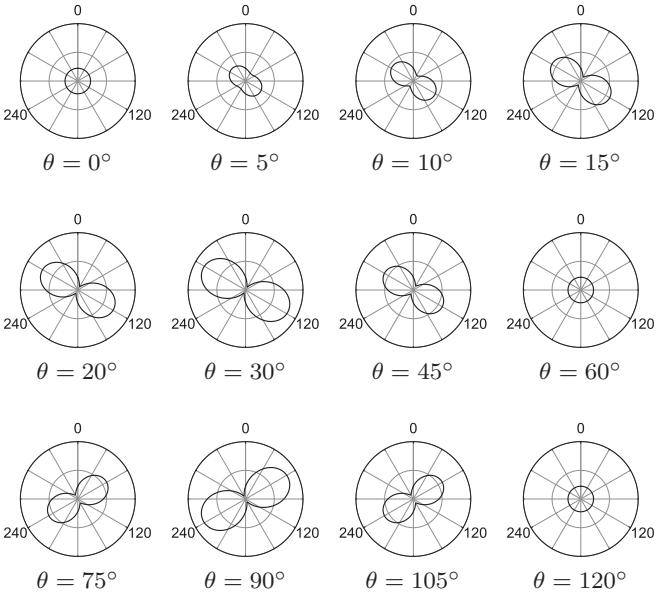

FIG. 3. Calculated intensity polar patterns of the TO mode under perpendicular analysis (⊥) for different rotation angles θ for a zinc-blende nanowire oriented along $\phi = 0°$. The patterns present a periodicity of 120° and are independent of ϕ for $\theta = 0°, 60°, 120°$.

approximately twice as large as the one for the wurtzite structure.[21,22] This leads to new allowed Raman modes that belong to the A_1, E_1, E_2^H, and E_2^L (H for high and L for low frequency) representations. At the Γ point, the modes A_1 and E_1 originate from a broken degeneracy due to the hexagonal symmetry compared to the cubic one while the E_2 mode "emerges" from the folding. Due to its symmetry, the I_s for wurtzite nanowires grown in the [0001] direction does not present any dependence on θ. In Fig. 4, the calculated polar patterns of the A_1 (TO), E_1 (TO), and E_2 modes are shown. For the polar A_1 (TO) mode, the strongest values of I_s are obtained in the parallel configurations [$x(y,y)\bar{x}$, $x(z,z)\bar{x}$, using Porto's notation[23]], i.e., when the incident and scattered light polarizations are parallel to each other. On the contrary, the polar E_1 (TO) mode is strongest in perpendicular configurations, where the incident and scattered light polarizations are perpendicular to each other [$x(y,z)\bar{x}$, $x(z,y)\bar{x}$]. The E_2 mode is forbidden for any configuration but $x(y,y)\bar{x}$. Here, the incident and the scattered light polarizations are perpendicular to the wire axis. Furthermore, no LO phonon is allowed.

In addition to the symmetry considerations discussed so far, we have also calculated the phonon dispersion for

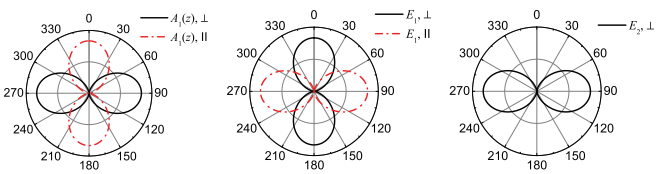

(a) A_1(TO) mode (b) E_1(TO) mode (c) E_2 mode

FIG. 4. (Color online) Calculated intensity polar patterns of the wurtzite modes for a nanowire oriented along $\phi = 0°$. The E_2 intensity is zero for parallel analysis (∥). While the maximum intensity for the A_1 mode is obtained in parallel configurations, the highest intensity of the E_1 mode is achieved for crossed polarizations.

TABLE I. Optical phonon modes in wurtzite InAs calculated using an extended 11-parameter rigid-ion model.

WZ mode	E_1 (LO)	A_1 (LO)	E_1 (TO)	A_1 (TO)	E_2^H	E_2^L
ν (cm^{-1})	246.8	246.3	226.0	225.5	219.2	43.6

the InAs wurtzite structure using an extended 11-parameter rigid-ion model.[24] This method allows us to calculate the phonons in a wurtzite structure parametrizing a known phonon dispersion relation of a zinc-blende structure. Thus, we fitted the experimental phonon dispersion data of zinc-blende InAs from Ref. 25 and calculated the phonon dispersion as well as the two-phonon density of states of the wurtzite structure. The obtained optical phonon modes at the Γ point of the wurtzite structure are presented in Table I. Note that the calculated values of the phonon energies are supposed to be higher than the experimental Raman phonon energies since the fitting of the zinc-blende data[25] obtained by x-ray thermal diffuse scattering exhibits ∼7–9 cm higher phonon energies than the zinc-blende InAs Raman data.[26]

These results show that the calculated E_2^H mode is similar in energy to the A_1 (TO) and E_1 (TO) modes. The slight splitting between the E_2^H and the A_1 (TO) mode is only 6.3 cm^{-1}. This is expected due to the fact that the TO phonon dispersion along the [111] direction of the zinc-blende structure is nearly horizontal.[25]

B. Polarization-dependent Raman scattering on InAs nanowires

In this subsection, we present the experimental polarized Raman scattering results from an individual InAs nanowire, which are compared with the theoretical considerations presented before. All measurements were performed in a backscattering configuration (see Fig. 1) where the wave vectors of the incident and scattered light (k_i, k_s) are perpendicular to the wire axis of the nanowire. A typical Raman spectrum in the $x(y,y)\bar{x}$ configuration is shown in Fig. 5. In addition, the clearly visible TO and LO mode, an SO mode, which will be discussed later, also appears.

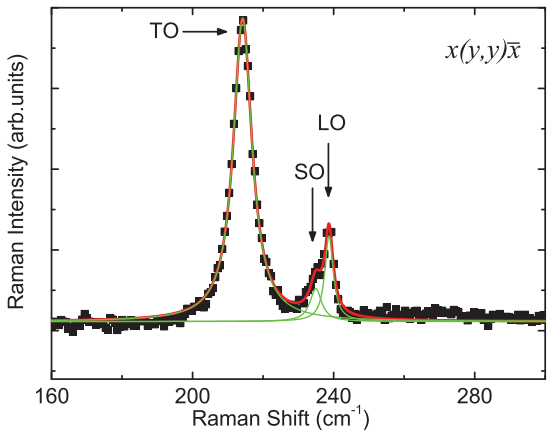

FIG. 5. (Color online) Typical Raman spectrum in an $x(y,y)\bar{x}$ configuration from an InAs nanowire using the 514.5 nm excitation line. An SO mode appears in addition to the TO and LO mode.

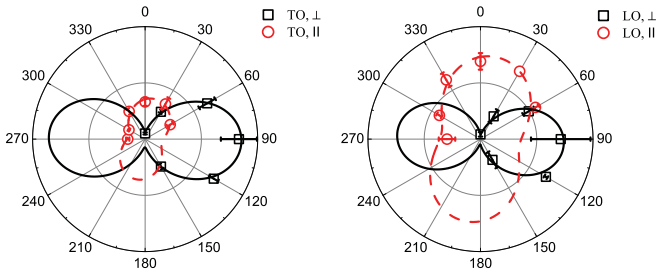

(a) TO mode (b) LO mode

FIG. 6. (Color online) Experimental polar patterns for the TO (a) and LO (b) mode for a nanowire grown at 480 °C and an excitation line of 514.5 nm. Solid and dashed curves are $\cos^2(\phi)$ fits to the data. ϕ denotes the angle between the polarization of the incident light and the nanowire axis. Open squares and circles represent the perpendicular and parallel analysis of the scattered light with respect to the nanowire axis (oriented along $\phi = 0°$). The standard deviation of at least three measurements is used as error bars.

All measured spectra were fitted with Lorentzian functions after the removal of the background contribution. The standard deviation of at least three measurements is used as an error bar. Although the experimental linewidth of the TO mode (∼6–13 cm^{-1}) is too large for a direct identification of the different modes, the detailed polarization dependence analysis performed provides useful information in this regard. In Fig. 6, the polar pattern of an InAs nanowire with the 514.5 nm excitation line for the TO mode (a) and the LO mode (b) is displayed. The TO (LO) mode intensities, $I_\perp$ and $I_\parallel$, are normalized to the highest observed TO (LO) mode intensity under perpendicular analysis. The measured TO mode intensities are a factor of 10 higher than the LO intensities. The measurements shown in Fig. 6(a) reveal that the TO mode is detected much stronger in parallel configurations $[x(y,y)\bar{x}, x(z,z)\bar{x}]$, i.e., when the incident and the scattered light polarizations are parallel to each other. Additionally, the observed intensity in $x(y,y)\bar{x}$ configuration is much higher than in the $x(z,z)\bar{x}$ configuration. These results are in accordance with the calculated polar patterns for the A_1 (TO) and E_2 modes shown in Figs. 4(a) and 4(c), respectively. Therefore, we attribute the measured TO signal to the combined signal coming from the A_1 (TO) and E_2^H modes. Note that the maximum Raman intensity for $I_\perp$ is higher than for $I_\parallel$ since for $I_\perp$ both modes contribute to the Raman signal [solid curves in Figs. 4(a) and 4(c)] while for $I_\parallel$ only the A_1 (TO) mode accounts for the polar pattern [dashed curve in Fig. 4(a)]. Furthermore, the E_1 (TO) mode, which theoretically contributes in crossed polarization configurations, does not appear in our experiments.

The polarization dependence of the much less pronounced LO peak shown in Fig. 6(b) also displays maximum intensities for detection under parallel configurations $[x(y,y)\bar{x}, x(z,z)\bar{x}]$. Taking into account only the symmetry of the wurtzite structure, the LO mode should not be present in our backscattering experiments. We attribute the breaking of this selection rule to the fact that in these measurements, the excitation energy (2.41 eV) is in the vicinity of the E_1 electronic transition of the wurtzite structure. As we will see in Sec. V, the E_1 transition of the investigated nanowire is redshifted by 100 meV from the bulk value (2.57 eV). Note that both TO and LO modes resonate, although the LO modes are more sensitive to the resonance due to the Fröhlich interaction, as expected.[19] This can be seen in the sharpness of the resonance (Fig. 10) and also in the ratio of the integrated peak intensities LO/TO, which is larger when the excitation energy of the photons is closer to the electronic resonance. Comparing the LO/TO ratio in the nanowire and the bulk, we obtain a twice as large value for the former one.

We believe that a contribution to the Raman signal coming from the zinc-blende portions of the nanowire, although it cannot be completely ruled out in both the TO and LO peaks, is only marginal. For instance, for cubic GaAs nanowires grown in the [111] direction, it was reported that the TO Raman signal is much stronger for the $x(z,z)\bar{x}$ than any other configuration.[13] This suggests that the contribution of the zinc-blende structure is weak and may only contribute in the $x(z,z)\bar{x}$ configuration, which, in our case, is partly a factor of 2 weaker than the $x(y,y)\bar{x}$ configuration.

C. Surface optical phonon in InAs nanowires

Surface optical phonons have been studied in thin films[27] and microcrystals,[28] and, recently, more attention has been devoted to nanowires. It has been showed that the shape (diameter[29] and cross section[30]) of the nanowire, the surrounding medium,[31] and the defect density[32] of the nanowire influences the SO mode. Thus, the SO mode shifts to lower wave numbers when decreasing the diameter of the nanowire.

As mentioned before in Fig. 5, a third mode at the low-energy side of the LO mode can be observed and is assigned to the SO mode of InAs nanowires due to the localization in one dimension.[32,33] A polarized Raman study on this mode reveals that it only appears in parallel configuration $x(y,y)\bar{x}$ where the incident and scattered light polarizations are perpendicular to the wire axis [Fig. 7(b)]. Although the polar pattern resembles the one for the E_2 mode presented earlier [see Fig. 4(c)], the E_2 mode can be excluded since its energy (see Table I) is well below the energy of the SO mode ($\omega_{SO} = 235.3$ cm^{-1}) observed in our measurements. A possible contribution due to two-phonon processes can be ruled out as well because of the low two-phonon density of states (DOS) at this frequency [see Fig. 7(a)]. The one-phonon DOS (not shown), which could be important under disorder, also does not present any relevant feature at this frequency. The densities of states were calculated using the extended 11-parameter rigid-ion model presented before. Altogether, the evidence we have observed and discussed here supports the attribution of this shoulder to an SO mode, although further experiments would be helpful to achieve a completely unambiguous identification. For instance, a definitive experiment would be the measurement of the Raman spectrum with the nanowire surrounded by different dielectric media in which this feature should be shifted.

Data are scarce regarding polarized Raman scattering on SO phonons. An SO study of a close-packed 2D array of CdSe nanorods reveals a suppression of the SO phonon when the incident light polarization is perpendicular to the wire axis.[34] This is explained by the modification of the dielectric surrounding due to the closed packing of the nanowires, different from the single nanowire study presented here. In wurtzite GaAs needles, an SO phonon has been proposed in $x(y,y)\bar{x}$ and

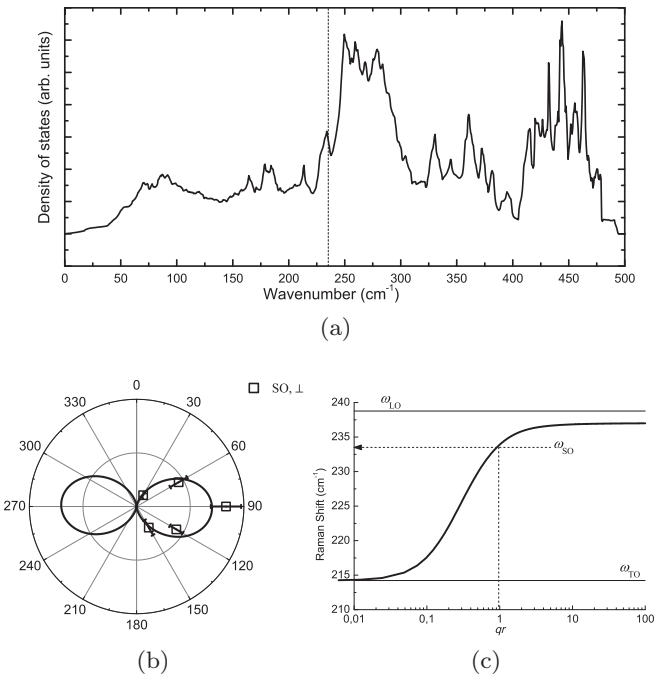

FIG. 7. (a) Two-phonon density of states (DOS) of wurtzite InAs calculated with an extended 11-parameter rigid-ion model. The dashed line represents the energy of the SO mode observed in our measurements. (b) Experimental polar pattern for the SO mode for an InAs nanowire. The solid curve is a $\cos^2(\phi)$ fit to the data. ϕ denotes the angle between the polarization of the incident light and the nanowire axis. Open squares represent the perpendicular analysis of the scattered light with respect to the nanowire axis. The standard deviation of at least three measurements is used as error bars. (c) Calculated dispersion relation ω_{SO} of the SO mode for an InAs nanowire. The horizontal lines represent the TO and LO modes at the zone center and the dashed line denotes the experimental SO frequency.

$x(z,y)\bar{x}$ configurations, but it could not be resolved.[14] From individual GaP nanowires, it is observed that the SO phonon appears strongest in the $x(y,y)\bar{x}$ configuration,[35] which is in agreement with our observations.

For an infinitely long cylindrical nanowire, the dispersion relation $\omega_{SO}(q)$ for the SO mode in the limit ($q \gg \omega/c$) can be written as follows:[31]

$$\omega_{SO}^2 = \omega_{TO}^2 + \frac{\tilde{\omega}_p^2}{\epsilon_\infty + \epsilon_m f(x)}, \quad x = qr, \tag{7}$$

where $\tilde{\omega}_p$ is the screened ion plasma frequency given by $\omega_{LO}^2 = \omega_{TO}^2 + \tilde{\omega}_p/\epsilon_\infty$, r is the radius of the nanowire, ϵ_∞ is the high-frequency dielectric constant of bulk InAs, and

$$f(x) = \frac{I_0(x)K_1(x)}{I_1(x)K_0(x)}, \tag{8}$$

where I and K are the modified Bessel functions. The calculated dispersion relation ω_{SO} as a function of qr is plotted in Fig. 7(c) considering $q = 2k = 4\pi/\lambda_L$ in backscattering geometry. For the case of InAs nanowires, we used $\epsilon_\infty = 12.25$,[36] $\epsilon_m = 1$ (air), and $\lambda_L = 514.5$ nm (laser wavelength). If we assume the nanowire diameter 70–80 nm measured by AFM, we obtain the SO energy $\omega_{SO} = 233.5 \pm 0.3$ cm^{-1},

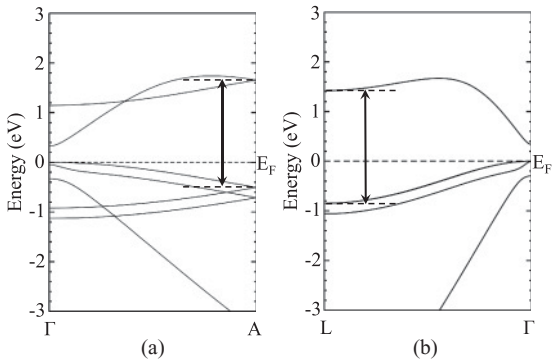

FIG. 8. *Ab initio* calculations of the electronic band structure of wurtzite (a) and zinc-blende (b) InAs along the directions $\Gamma-A$ and $\Gamma-L$, respectively. The arrows denote the electronic transition energies at the corresponding symmetry points.

which is slightly higher than the energy observed experimentally (235.3 ± 0.5 cm^{-1}).

V. RESONANT RAMAN SCATTERING IN SINGLE InAs NANOWIRES

It is predicted that the electronic band structure of the zinc-blende structure of InAs is different from the wurtzite structure of the same material,[3,4] which leads to different transition energies. Focusing on the E_1 transition of InAs, we employed the WIEN2K code[37] to perform *ab initio* calculations of the electronic band structure along the [0001] growth direction of the wurtzite phase [from Γ to A, Fig. 8(a)] and of the band structure along the [111] growth direction of the zinc-blende phase [from Γ and L, Fig. 8(b)]. The arrows in Fig. 8 denote the energy separation at the corresponding symmetry points. It is worth noting that in these calculations, a modified Becke-Johnson (mBJ) potential[38] has been used, providing a more reliable value for the empty states as compared with the calculations reported in Ref. 39. The calculations reveal for the zinc-blende structure a transition energy of approximately 110 meV larger than for the wurtzite structure. Since the E_1 transition of the cubic crystal structure is close to the L point, we expect that the transition energy in the wurtzite structure is smaller.

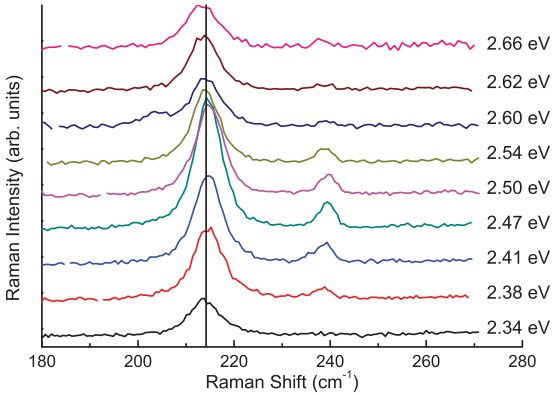

FIG. 9. (Color online) Series of Raman spectra from an InAs nanowire measured as a function of the laser energy. A resonance enhancement of the TO and LO mode is clearly visible.

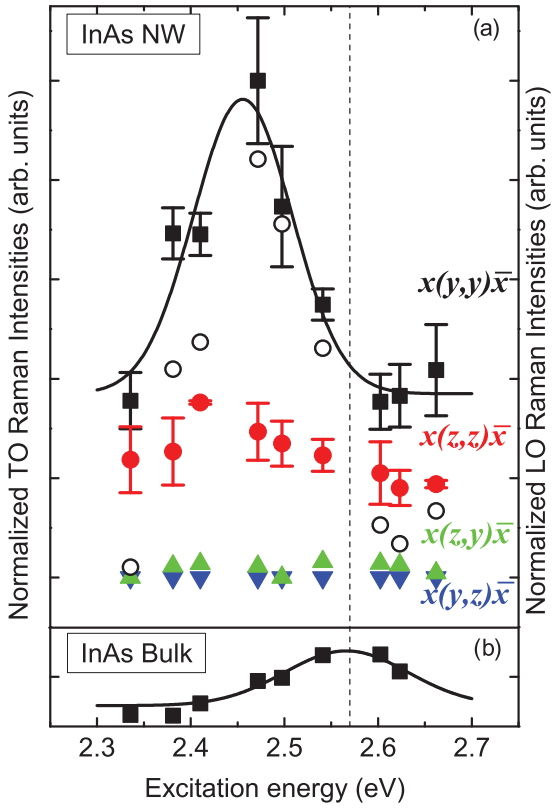

FIG. 10. (Color online) (a) Integrated resonant Raman intensities of the TO modes (filled symbols) from an InAs nanowire as a function of the laser excitation energy for the four main polarization configurations. The open circles correspond to the integrated Raman intensities of the LO modes measured for the $x(y,y)\bar{x}$ configuration. The standard deviation of at least three measurements is used as error bars. (b) Reference measurement from InAs bulk material.

Resonant Raman scattering was measured to determine the E_1 transition energies. Our measurements were performed with nine lines of the Ar/Kr ion laser (2.34–2.66 eV) on the same nanowire investigated in the preceding section. A series of Raman spectra, measured as a function of the laser excitation energy, is shown in Fig. 9. The spectra were taken in a parallel polarization configuration $x(y,y)\bar{x}$. All spectra were corrected according to the ω^4 law [Eq. (1)]. Two modes at 214 cm^{-1} (TO) and 239 cm^{-1} (LO) can be clearly identified. Figure 10(a) shows for the four main polarization configurations $x(y,y)\bar{x}$, $x(y,z)\bar{x}$, $x(z,y)\bar{x}$, and $x(z,z)\bar{x}$ the integrated Raman intensities of the TO mode as a function of the laser energy. In addition, the integrated Raman intensities of the LO mode in the $x(y,y)\bar{x}$ configuration (open circles) are presented. The data were corrected with respect to the different responses of the grating and the beam splitter due to the different polarizations and incident laser excitation wavelengths λ_L. The error bars in Fig. 10(a) represent the standard deviation of different measurements after new alignment on the same spot of the nanowire. For the parallel polarization configurations $[x(y,y)\bar{x}, x(z,z)\bar{x}]$, an enhancement of the Raman scattering intensity with a maximum at 2.47 eV (Gaussian fit) is observed. This is consistent with the polarization-dependent Raman scattering results given in the preceding section, where the maximum intensities are obtained for parallel configurations. Figure 10(b) shows as a reference the resonant Raman scattering from zinc-blende InAs bulk with a peak at 2.57 eV, in agreement with previous publications.[40–43] The resonance energy obtained experimentally for the nanowire is redshifted as compared to the one obtained for the bulk zinc-blende InAs. This is in qualitative agreement with the *ab initio* calculated E_1 transition energies for the zinc-blende and wurtzite structures that indicate a lower E_1 transition energy for the latter.

The integrated Raman intensities of the LO mode lead to the same result [open circles in Fig. 10(a)]. However, due to the reduced signal intensity (~ 0.25 counts/s in resonance), the LO phonon can mostly be observed in the $x(y,y)\bar{x}$ configuration and disappears far from resonance (see Fig. 9). Confinement or strain effects can be neglected due to the large diameter of the nanowire.

VI. CONCLUSIONS

We have performed polarized Raman scattering on single InAs nanowires. The polarization dependence of the TO and LO modes has been determined. The highest intensity for the TO mode is obtained in the $x(y,y)\bar{x}$ configuration, where the incident and scattered polarizations are parallel to each other and perpendicular to the nanowire axis. Here, the contribution to the Raman signal comes from the wurtzite A_1 (TO) and E_2 modes, which is in good agreement with calculations of the wurtzite phonon energies using an extended rigid-ion model. Resonant Raman scattering on the same nanowire reveals a redshifted E_1 transition with respect to the electronic E_1 transition of zinc-blende bulk InAs. This shift is a consequence of the wurtzite structure in the nanowires, which is supported by an *ab initio* calculation of the electronic band structure for wurtzite and zinc-blende structure.

ACKNOWLEDGMENTS

We thank the Spanish Ministry of Science and Innovation (Grants No. TEC2009-12075 and No. MAT2009-10350) as well as CNPq, CAPES, and FAPESP for financial support and the University of Valencia for the computing facilities. We also acknowledge LNLS, Brazil, for granting access to the electron microscopy facilities.

*michael.moeller@uv.es

[1] W. Lu and C. M. Lieber, Nat. Mater. **6**, 841 (2007).
[2] P. Yang, R. Yan, and M. Fardy, Nano Lett. **10**, 1259 (2010).
[3] Z. Zanolli, F. Fuchs, J. Furthmüller, U. von Barth, and F. Bechstedt, Phys. Rev. B **75**, 245121 (2007).
[4] A. De and C. E. Pryor, Phys. Rev. B **81**, 155210 (2010).

[5]K. Tomioka, J. Motohisa, S. Hara, and T. Fukui, Nano Lett. **8**, 3475 (2008).
[6]K. A. Dick, Prog. Cryst. Growth Charact. Mater. **54**, 138 (2008).
[7]K. Hiruma, M. Yazawa, T. Katsuyama, K. Ogawa, K. Haraguchi, M. Koguchi, and H. Kakibayashi, Appl. Phys. Rev. **77**, 447 (1995).
[8]H. Shtrikman, R. Popovitz-Biro, A. Kretinin, L. Houben, M. Heiblum, M. Bukala, M. Galicka, R. Bucko, and P. Kacman, Nano Lett. **9**, 1506 (2009).
[9]H. J. Joyce, J. Wong-Leung, Q. Gao, H. Hoe Tan, and C. Jagadish, Nano Lett. **10**, 908 (2010).
[10]K. A. Dick, C. Thelander, L. Samuelson, and P. Caroff, Nano Lett. **10**, 3494 (2010).
[11]T. Livneh, J. Zhang, G. Cheng, and M. Moskovits, Phys. Rev. B **74**, 035320 (2006).
[12]E. O. Schäfer-Nolte, T. Stoica, T. Gotschke, F. Limbach, E. Sutter, P. Sutter, and R. Calarco, Appl. Phys. Lett. **96**, 091907 (2010).
[13]I. Zardo, S. Conesa-Boj, F. Peiro, J. R. Morante, J. Arbiol, E. Uccelli, G. Abstreiter, and A. Fontcuberta i Morral, Phys. Rev. B **80**, 245324 (2009).
[14]S. Crankshaw, L. C. Chuang, M. Moewe, and C. Chang-Hasnain, Phys. Rev. B **81**, 233303 (2010).
[15]J. Wu, D. Zhang, Q. Lu, H. R. Gutierrez, and P. C. Eklund, Phys. Rev. B **81**, 165415 (2010).
[16]C.-T. Chien, M.-C. Wu, C.-W. Chen, H.-H. Yang, J.-J. Wu, W.-F. Su, C.-S. Lin, and Y.-F. Chen, Appl. Phys. Lett. **92**, 223102 (2008).
[17]M. H. Kim, J. M. Baik, S. J. Lee, H.-Y. Shin, J. Lee, S. Yoon, G. D. Stucky, M. Moskovits, and A. M. Wodtke, Appl. Phys. Lett. **96**, 213108 (2010).
[18]H. M. Fan, Z. H. Ni, Y. Feng, X. F. Fan, J. L. Kuo, Z. X. Shen, and B. S. Zou, Appl. Phys. Lett. **91**, 171911 (2007).
[19]P. Y. Yu and M. Cardona, *Fundamentals of Semiconductors* (Springer, Berlin, New York, 2005).
[20]R. M. Martin and T. C. Damen, Phys. Rev. Lett. **26**, 86 (1971).
[21]J. L. Birman, Phys. Rev. **115**, 1493 (1959).
[22]J. Zi, X. Wan, G. Wei, K. Zhang, and X. Xie, J. Phys. Condens. Matter **8**, 6323 (1996).
[23]T. C. Damen, S. P. S. Porto, and B. Tell, Phys. Rev. **142**, 570 (1966).
[24]J. R. Madureira and A. Cantarero (unpublished).
[25]N. S. Orlova, Phys. Status Solidi B **119**, 541 (1983).
[26]R. Carles, N. Saint-Cricq, J. B. Renucci, M. A. Renucci, and A. Zwick, Phys. Rev. B **22**, 4804 (1980).
[27]S. Ushioda, A. Aziza, J. B. Valdez, and G. Mattei, Phys. Rev. B **19**, 4012 (1979).
[28]S. Hayashi and H. Kanamori, Phys. Rev. B **26**, 7079 (1982).
[29]D. Spirkoska, G. Abstreiter, and A. Fontcuberta i Morral, Nanotechnol. **19**, 435704 (2008).
[30]K. W. Adu, Q. Xiong, H. R. Gutierrez, G. Chen, and P. C. Eklund, Appl. Phys. A **85**, 287 (2006).
[31]R. Gupta, Q. Xiong, G. D. Mahan, and P. C. Eklund, Nano Lett. **3**, 1745 (2003).
[32]N. Begum, A. S. Bhatti, F. Jabeen, S. Rubini, and F. Martelli, J. Appl. Phys. **106**, 114317 (2009).
[33]M. Cantoro, A. V. Klekachev, A. Nourbakhsh, B. Sorée, M. M. Heyns, and S. De Gendt, Eur. Phys. J. B **79**, 423 (2011).
[34]C. Nobile, V. A. Fonoberov, S. Kudera, A. Della Torre, A. Ruffino, G. Chilla, T. Kipp, D. Heitmann, L. Manna, R. Cingolani, A. A. Baladin, and R. Krahne, Nano Lett. **7**, 476 (2007).
[35]Q. Xiong, G. Chen, H. R. Gutierrez, and P. C. Eklund, Appl. Phys. A **85**, 299 (2006).
[36]*Semiconductors—Basic Data*, edited by O. Madelung (Springer, Berlin, 1996).
[37]P. Blaha, K. Schwarz, K. H. Madsen, D. Kvasnicka, and J. Luitz, in *WIEN2k, An Augmented Plane Wave + Local Orbitals Program for Calculating Crystal Properties*, edited by K. Schwarz (Technische Universität Wien, Austria, 2001).
[38]F. Tran and P. Blaha, Phys. Rev. Lett. **102**, 226401 (2009).
[39]M. Möller, L. C. O. Dacal, M. M. J. de Lima, T. Chiaramonte, M. A. Cotta, F. Iikawa, and A. Cantarero (in press).
[40]R. C. C. Leite and J. F. Scott, Phys. Rev. Lett. **22**, 130 (1969).
[41]M. A. Renucci, J. B. Renucci, and M. Cardona, Phys. Status Solidi B **49**, 625 (1972).
[42]R. Carles, N. Saint-Cricq, J. B. Renucci, A. Zwick, and M. A. Renucci, Phys. Rev. B **22**, 6120 (1980).
[43]T. Angelova, A. Cros, A. Cantarero, D. Fuster, Y. González, and L. González, J. Appl. Phys. **104**, 033523 (2008).